

# Topological Magnetic Excitations on the Distorted Kagomé Antiferromagnets: Applications to Volborthite, Vesignieite, and Edwardsite.

S. A. Owerre<sup>1,2</sup>

<sup>1</sup>*Perimeter Institute for Theoretical Physics, 31 Caroline St. N., Waterloo, Ontario N2L 2Y5, Canada.*

<sup>2</sup>*African Institute for Mathematical Sciences, 6 Melrose Road, Muizenberg, Cape Town 7945, South Africa.*

Inelastic neutron scattering experiment has uncovered a finite thermal Hall conductivity on the frustrated distorted kagomé volborthite at nonzero magnetic field with no signal of Dzyaloshinskii-Moriya (DM) spin-orbit interaction. The observed thermal Hall response is attributed to an emergence of nontrivial elementary excitations. However, the origin of the nontrivial topological magnetic excitations and the associated thermal Hall response has not been identified unlike in collinear unfrustrated magnets where it is well established that the DM interaction is the driving force. Several distorted kagomé antiferromagnets, such as vesignieite, edwardsite, and volborthite show evidence of magnetically ordered phases at low temperatures. Here, we identify a chiral spin order on the distorted kagomé-lattice antiferromagnets which is not induced by the DM interaction, but by a topological noncoplanar spin texture due to the presence of a magnetic field applied perpendicular to the distorted kagomé plane. The noncoplanar magnetic spin texture has a nonzero scalar spin chirality similar to a chiral quantum spin liquid with broken time-reversal symmetry. In the noncoplanar regime, we observe nontrivial topological magnetic excitations even without the DM interaction. The associated Hall response is termed “topological” thermal Hall effect as it originates from the real space Berry curvature of the spin texture rather than the DM spin-orbit interaction.

## I. INTRODUCTION

Thermal Hall measurement is the new avenue of probing nontrivial topological magnetic excitations in insulating quantum magnets [1–3]. For ordered quantum magnets, the magnetic excitations are magnons and the corresponding Hall effect is dubbed magnon Hall effect (MHE) [1, 2, 4–9]. Thermal Hall response has been realized in the collinear kagomé ferromagnet Cu(1-3, bdc) [2] and previously observed in a number of collinear pyrochlore ferromagnets [1, 6]. An interesting feature of these systems is that they host topological magnon dispersions (TMDs) [4, 5, 7–9, 11–14], induced by the DM interaction [15] which originates from spin-orbit coupling (SOC) [16]. Thus, they are dubbed topological magnon insulators (TMI) for two-dimensional (2D) systems [7, 9] and Weyl magnon (WM) for 3D systems [12, 13] similar to electronic counterparts [17–21]. Recently, TMI and MHE have been proposed in collinear honeycomb ferromagnets [22–24].

The Heisenberg antiferromagnet on the kagomé lattice with corner-sharing equilateral triangles is a non-bipartite frustrated system. Classically, the ground state exhibits an extensive degeneracy and it is believed that quantum fluctuations lift these classical degenerate ground states via order-by-disorder mechanism [25, 26], and a coplanar/noncollinear 120° pattern with a  $\mathbf{Q} = \mathbf{0}$  propagation vector is selected, which is stabilized by either a second nearest-neighbour antiferromagnetic interaction [26] or an out-of-plane DM interaction [27–34]. In realistic kagomé materials, the DM interaction is an intrinsic anisotropy, because by the Moriya rules [16] the midpoint of the bonds connecting two magnetic ions on the kagomé lattice is not an inversion center. Various experimentally accessible kagomé antiferromagnetic materials such as iron

jarosites [28–30], vesignieite  $\text{BaCu}_3\text{V}_2\text{O}_8(\text{OH})_2$  [35–39], edwardsite  $\text{Cd}_2\text{Cu}_3(\text{SO}_4)_2(\text{OH})_6 \cdot 4\text{H}_2\text{O}$  [40], and volborthite  $\text{Cu}_3\text{V}_2\text{O}_7(\text{OH})_2 \cdot 2\text{H}_2\text{O}$  [41–43] have long-range magnetic orders at certain temperatures. They are generally attributed to the presence of DM interaction.

Although extensive studies have been investigated for unfrustrated collinear magnets both theoretically [4–9, 11–14, 22–24] and experimentally [1, 2, 6, 10], the study of nontrivial topological magnetic excitations and the associated thermal Hall effect in geometrically frustrated magnets has been completely neglected. The lack of intensive study of topological magnetic excitations in geometrically frustrated magnets is probably due to the fact that the DM interaction does not play the same topological role as in unfrustrated collinear magnets. In a recent experimental report [3], a nonzero thermal Hall conductivity ( $\kappa_{xy}$ ) has been observed in a frustrated distorted kagomé volborthite, at a strong magnetic field of 15 T and no discernible Hall signal was observed at zero magnetic field [44]. The authors attributed the presence of  $\kappa_{xy}$  to nontrivial elementary excitations in the gapless quantum spin liquid (QSL) phase, however a strong field of 15 T is sufficient to cause magnetic phases in volborthite at least in the low temperature regime [42, 43, 45]. Nevertheless, we do not know the exact nature of the magnetically ordered phases at 15 T, but the intrinsic DM anisotropy suggests a  $\mathbf{Q} = \mathbf{0}$  coplanar/noncollinear Néel order.

The exact spin Hamiltonian that describes kagomé volborthite has been very controversial. Attempts to describe previous experimental features of volborthite have led to different proposals of spin Hamiltonian which include: coupled frustrated chains [46, 47], coupled trimers [48], and anisotropic Heisenberg exchange model [49–52]. In this paper, we will adopt the latter model. Indeed, the experimental observation of  $\kappa_{xy}$  in volborthite dif-

fers significantly from collinear ferromagnets as the system is frustrated. Previously, it has been conjectured that the thermal Hall effect is present in frustrated magnets due to a Lorentz force in the deconfined fermionic spinons coupled to an emergent gauge field [4]. In principle, the charge-neutral magnetic excitations should not feel a Lorentz force and the DM interaction and external magnetic field have a profound effect on frustrated magnets which have not been taken into account. Therefore the mechanism that gives rise to a nonzero thermal Hall effect in insulating frustrated magnets is still an open question. The main goal of this paper is to address this question. That is *if the observed  $\kappa_{xy}$  in volborthite is due to topological magnon in the magnetic-field-induced phases or nontrivial elementary excitations in the gapless QSL phases, what is the origin of the topological magnetic excitations that give rise to a nonzero thermal Hall conductivity in volborthite?*

## II. MODEL

We consider the generic spin Hamiltonian on the distorted kagomé antiferromagnets subject to a magnetic field perpendicular to the kagomé plane. The Hamiltonian is given by

$$\mathcal{H} = \sum_{ij} [J_{ij} \mathbf{S}_i \cdot \mathbf{S}_j + \mathbf{D}_{ij} \cdot \mathbf{S}_i \times \mathbf{S}_j] - \mathbf{H} \cdot \sum_i \mathbf{S}_i, \quad (1)$$

where  $\mathbf{S}_i$  is the magnetic spin moment at site  $i$ ,  $J_{ij} = J > 0$  on the diagonal bonds and  $J_{ij} = J' = J\delta$  on the horizontal bonds with  $\delta \neq 1$  as shown in Fig. 1. The inversion symmetry breaking on the kagomé lattice allows a DM vector  $\mathbf{D}_{ij} = -D_{\perp} \hat{\mathbf{z}}$  and they lie at the midpoints between two magnetic ions as shown in Fig. 1. The last term is the out-of-plane external magnetic field  $\mathbf{H} = h\hat{\mathbf{z}}$  and  $h = g\mu_B H$ . The out-of-plane DM interaction stabilizes the coplanar/noncollinear spin configuration [27]. In most kagomé materials an in-plane DM interaction  $D_{\parallel}$  may be present due to lack of mirror planes. It leads to weak out-of-plane ferromagnetism with small ferromagnetic moment. However, it is usually negligible compared to the out-of-plane component for most spin-1/2 kagomé antiferromagnetic materials [31, 32] and can be removed by gauge transformation. For kagomé volborthite [3], there was no signal of both in-plane and out-of-plane DM interaction on the observed  $\kappa_{xy}$ . Also, for potassium Fe-jaerosite with spin-5/2 the in-plane DM interaction (or the DM interaction in general) does not induce TMDs [30]. Therefore, we will neglect the small in-plane DM component at the moment and comment on its effects in the subsequent sections.

Let us start from what is known for distorted kagomé antiferromagnets at  $\mathbf{D}_{ij} = h = 0$  [51]. In this case, the

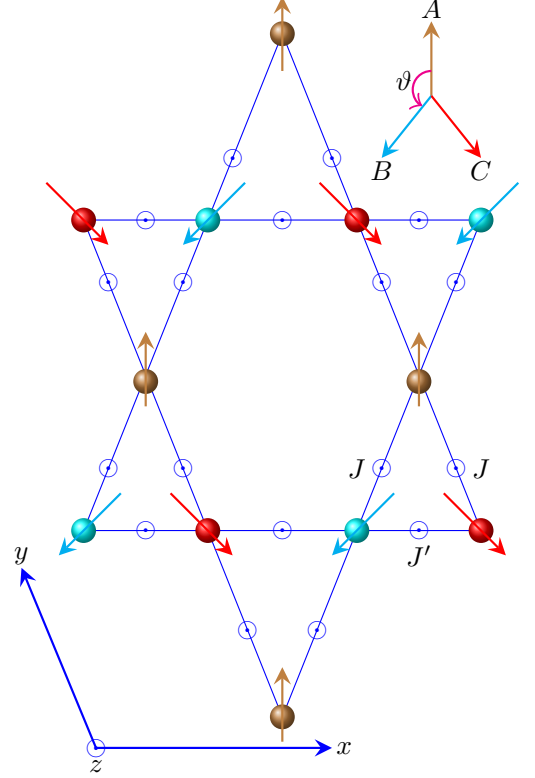


FIG. 1. Color online. Distorted kagomé lattice with canted coplanar/noncollinear magnetic order with positive vector chirality. The out-of-plane DM interaction lies at the midpoints between two magnetic ions as indicated by small dotted circles. The spin triad are separated by an angle  $\vartheta \neq 120^\circ$  on each isosceles triangle with  $J \neq J'$  as shown at the top figure.

Hamiltonian can be written as

$$\mathcal{H} = \frac{J\delta}{2} \sum_{\Delta} \left( \frac{1}{\delta} \mathbf{S}_A + \mathbf{S}_B + \mathbf{S}_C \right)^2 - \text{const.}, \quad (2)$$

where  $\mathbf{S}_{A,B,C}$  form a triad as depicted in Fig. 1. It is easily seen that the classical energy is minimized for  $\frac{1}{\delta} \mathbf{S}_A + \mathbf{S}_B + \mathbf{S}_C = 0$ , yielding  $\vartheta = \arccos(-1/2\delta) \neq 120^\circ$  for  $\delta \neq 1$ . The classical configuration is now a canted coplanar/noncollinear spins for  $\delta > 1/2$  [51]. However, it also has an extensive degeneracy as in the ideal kagomé Heisenberg antiferromagnets. There are several limiting cases in which the system is either bipartite with collinear magnetic order or non-bipartite with non-collinear magnetic order. The limiting case  $\delta \rightarrow 0$  maps to a bipartite square lattice with collinear magnetic order and  $\delta \rightarrow \infty$  maps to a decoupled antiferromagnetic chains. For  $\delta < 1/2$  it has been established that the classical ground state is collinear (up-down-down state) and there is no degeneracy except a global spin rotation about the  $z$ -axis, and for  $\delta > 1/2$  the classical ground state is non-collinear but coplanar. The collinear phases are triv-

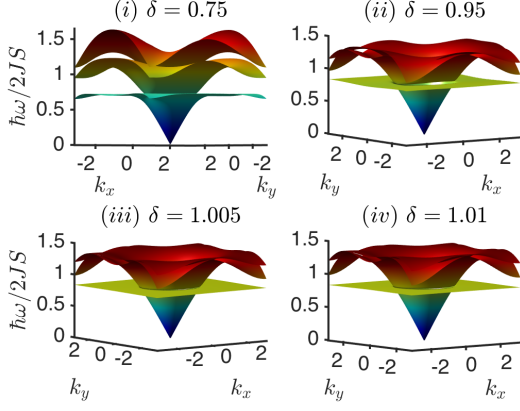


FIG. 2. Color online. Magnon dispersion of distorted kagomé antiferromagnet at zero magnetic field and several values of distortion with  $D_{\perp}/J = 0.2$ .

ial. In the present study, we focus on the canted coplanar/noncollinear regime ( $\delta > 1/2$ ) as the ground state properties of volborthite, vesignieite, and edwardsite are believed to live in this regime.

### III. CLASSICAL GROUND STATE

Now, we consider the classical ground state of the full Hamiltonian (1). In the classical limit, the spin operators can be approximated as classical vectors, written as  $\mathbf{S}_i = S\mathbf{n}_i$ , where  $\mathbf{n}_i = (\sin \phi \cos \theta_i, \sin \phi \sin \theta_i, \cos \phi)$  is a unit vector and  $\theta_i$  labels the spin oriented angles on the spin triad and  $\phi$  is the magnetic-field-induced canting angle. For  $\delta > 1/2$  the ground state is the canted coplanar/noncollinear spin configuration in Fig. 1. The classical energy is given by

$$e_0(\phi) = 2J(2 + \delta) \left[ (1 - \cos \vartheta) \cos^2 \phi + \cos \vartheta \right] - 4D_{\perp} \sin^2 \phi \sin \vartheta (1 - \cos \vartheta) - 3h \cos \phi, \quad (3)$$

where  $e_0(\phi) = E(\phi)/NS^2$ , and  $N$  is the number of sites per unit cell. The magnetic field is rescaled in unit of  $S$ . The minimization of  $e_0(\phi)$  yields the magnetic-field-induced canting angle  $\cos \phi = h/h_s$  where

$$h_s = \frac{(1 - \cos \vartheta)}{3} [4J(2 + \delta) + 8D_{\perp} \sin \vartheta]. \quad (4)$$

As can be seen from Eq. 3 the classical energy depends on the DM interaction as it contributes to the stability of the coplanar/noncollinear spin configuration. In collinear spin configurations, the DM interaction does not contribute to the classical energy, instead it provides TMDs, e.g. in kagomé ferromagnets [1, 2, 4–14].

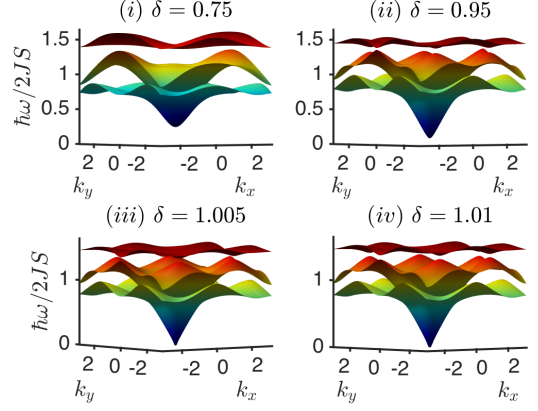


FIG. 3. Color online. Topological magnon dispersion of distorted kagomé antiferromagnet at finite magnetic-field-induced scalar spin chirality. The parameters chosen are  $h/h_s = 0.3$  and  $D_{\perp}/J = 0.2$ .

### IV. TOPOLOGICAL MAGNETIC EXCITATIONS

The magnetic excitations of frustrated kagomé antiferromagnets can be studied in different formalisms. In the present study, we use the large- $S$  expansion or the Holstein-Primakoff (HP) transformation [67] since we are interested in the low temperature regime. Moreover, the DM interaction and the magnetic field are very likely to induce a magnetic long-range order [42, 43, 45]. In the Supplemental material (SM), we have shown that a magnetic field ( $H \perp 2D$  plane) can induce a chiral noncoplanar spin texture with an emergent scalar spin chirality  $\chi_{ijk} = \cos \phi [\mathbf{S}_i \cdot (\mathbf{S}_j \times \mathbf{S}_k)]$ , where  $\cos \phi \propto H$ . The scalar spin chirality breaks time-reversal ( $\mathcal{T}$ ) symmetry macroscopically but preserves  $SU(2)$  symmetry. It is the hallmark of chiral spin liquid (CSL) [53–60] which also breaks  $\mathcal{T}$ -symmetry macroscopically. In the magnetic-field-induced noncoplanar regime the DM interaction is immaterial but the system still exhibits nontrivial topological effects through real space Berry curvature of the spin texture. This is reminiscent of topological Hall effect of charge particles in frustrated electronic systems [61–64]. The present model is, however, a charge-neutral excitation in a frustrated kagomé antiferromagnet. Evidently, this result sharply differs from magnetic-field-induced thermal Hall response in collinear honeycomb antiferromagnets with canted two-sublattice Néel ordered states [65] and triplon bands in a dimerized quantum magnet [66]. In these cases  $\chi_{ijk} = 0$ , therefore a nonzero thermal Hall response is induced by the DM interaction [65, 66].

In the present model, the magnetic excitations at zero magnetic field and zero DM interaction with  $\delta \neq 1$  still exhibit a zero energy mode  $\omega_1 = 0$  (not shown). The canted coplanar/noncollinear order due to lattice distortion is unable to lift the zero energy mode. In addition, there are two non-degenerate dispersive modes  $\omega_2 \neq \omega_3$

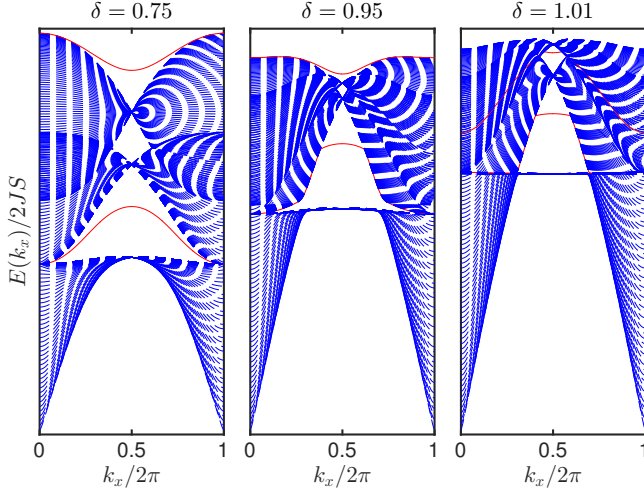


FIG. 4. Color online. Chiral magnon edge modes at zero magnetic field for a strip geometry on the distorted kagomé lattice with  $D_{\perp}/J = 0.2$ . The chiral edge modes are denoted by solid red lines.

(not shown) induced by lattice distortion in contrast to undistorted kagomé antiferromagnets with degenerate modes  $\omega_2 = \omega_3$ . Although the exact parameter values of volborthite are not known, an out-of-plane DM interaction is intrinsic to the kagomé lattice. A moderate DM interaction ( $D_{\perp}/J = 0.2$ ) lifts the zero energy mode and stabilizes the coplanar/noncollinear spin configuration as shown in Fig. 2. From symmetry point of view, the mirror reflection ( $\mathcal{M}$ ) symmetry is a good symmetry of the kagomé lattice, but it reverses the in-plane spins in the  $x$ - $y$  plane. Under  $\mathcal{T}$ -symmetry, the spins will be flipped again and return to the original state, hence  $\mathcal{TM}$  is a symmetry of the coplanar/noncollinear magnetic order. Since the lattice distortion and the out-of-plane DM interaction preserve this combined symmetry the system should be topologically trivial as we will show below. Therefore, we expect this model to be topologically non-trivial when either  $\mathcal{T}$ -symmetry or  $\mathcal{M}$ -symmetry is broken.

The combined symmetries can be broken in two ways. (i) If the kagomé lattice lacks  $\mathcal{M}$ -symmetry, an in-plane DM component  $D_{\parallel}$  might be present according to the Moriya rules [16]. The in-plane DM component preserves  $\mathcal{T}$ -symmetry but breaks  $\mathcal{M}$ -symmetry, hence  $\mathcal{TM}$  will be broken. This leads to weak out-of-plane ferromagnetism or noncoplanar spin canting with scalar spin chirality and weak ferromagnetic moment [27, 68]. Thus, for kagomé antiferromagnetic materials with  $D_{\perp} \ll D_{\parallel}$  we expect the out-of-plane ferromagnetism to be dominant and hence the (in-plane) DM interaction should be the primary source of topological spin excitations as we already know in collinear ferromagnets with out-of-plane DM interaction. However, most kagomé antiferromagnetic materials have a dominant intrinsic out-of-plane component  $D_{\perp} \gg D_{\parallel}$  and the weak ferromagnetism in-

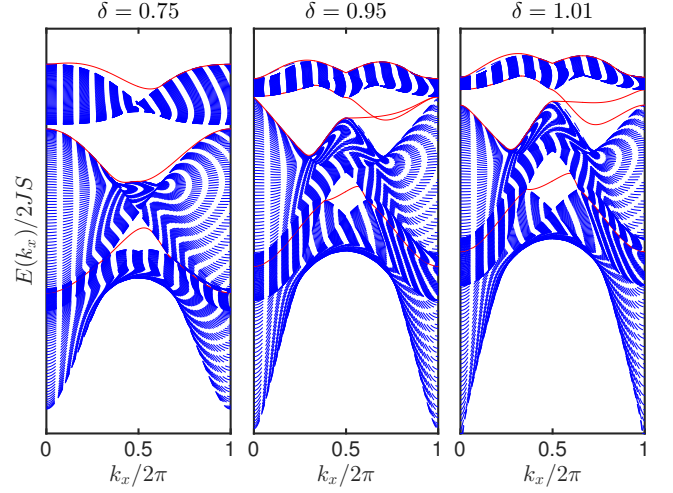


FIG. 5. Color online. Topological chiral magnon edge modes due to magnetic-field-induced scalar spin chirality. The parameters chosen are  $h/h_s = 0.3$  and  $D_{\perp}/J = 0.2$ . The chiral edge modes are denoted by solid red lines.

duced by  $D_{\parallel}$  can be negligible. In fact, there was no signal of any DM interaction on the observed  $\kappa_{xy}$  in kagomé volborthite [3]. Therefore, there must be another source of topological spin excitations apart from the DM interactions. (ii) An alternative way to break  $\mathcal{TM}$  symmetry is by applying an external magnetic field perpendicular to the kagomé plane ( $\mathbf{H} \perp 2\text{D plane}$ ). A finite out-of-plane magnetic field breaks  $\mathcal{T}$ -symmetry but preserves  $\mathcal{M}$ -symmetry. It induces a noncoplanar spin texture with a nonzero scalar spin chirality (see SM). The magnon dispersions are also gapped as depicted in Fig. 3 similar to the case without magnetic field. However, the gap excitations with and without the magnetic field are different which can be shown by solving for the chiral edge modes. The magnon edge modes for a strip geometry with open boundary conditions along the  $y$ -direction and infinite along  $x$ -direction are shown in Fig. 4 at zero magnetic field. We see that the system does not possess topologically protected gapless edge modes and the Chern number vanishes (see SM). On the other hand, the edge modes at finite magnetic field shown in Fig. 5 are gapless — an indication of a topological system. The magnetic-field-induced noncoplanar spin texture does not require a DM interaction in general. This is reminiscent of the experimental observation in kagomé volborthite [3]. We reiterate that the magnetic field can also lead to broken  $\mathcal{T}$ -symmetry in paramagnets and  $\chi_{ijk}$  is present in CSL phase of the kagomé antiferromagnets.

## V. TOPOLOGICAL THERMAL HALL EFFECT

Topological Hall effect is an unconventional Hall conductivity induced by the scalar spin chirality resulting from the configuration of the spin textures rather than

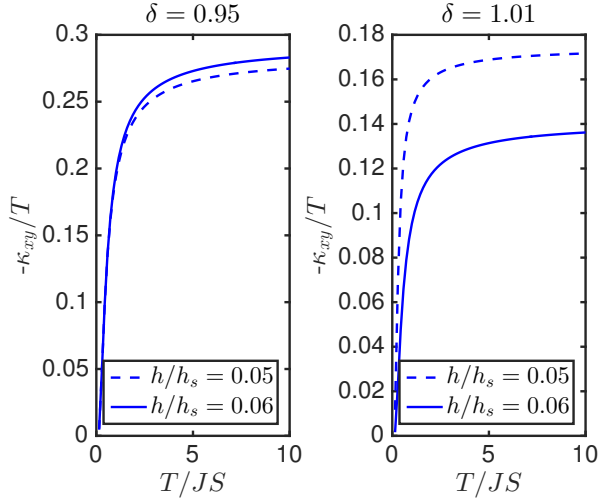


FIG. 6. Color online. Low temperature dependence of the topological thermal Hall conductivity with  $D_{\perp}/J = 0.2$ .

the spin-orbit interaction as reported in several electronic (metallic) systems [61–64]. In the present model the magnetic excitations are charge-neutral quasiparticles on the frustrated kagomé antiferromagnets. In this case the transverse Hall conductivity requires the presence of a temperature gradient  $-\nabla T$  which induces a heat current  $\mathcal{J}^Q$ . From linear response theory, one obtains  $\mathcal{J}_{\alpha}^Q = -\sum_{\beta} \kappa_{\alpha\beta} \nabla_{\beta} T$ , where  $\kappa_{\alpha\beta}$  is the thermal conductivity and the transverse component  $\kappa_{xy}$  is associated with the thermal Hall conductivity given explicitly in Ref. [69].

As expected from the analyses given above, there is no  $\chi_{ijk}$  at zero magnetic field and we find vanishing  $\kappa_{xy}$  despite distortion-induced gap magnon dispersion. This further confirms that the system is topologically trivial at zero field irrespective of the DM interaction. For finite magnetic field a nonzero scalar spin chirality is induced. Figure 6 shows the low temperature dependence of  $\kappa_{xy}$  (in units of  $k_B/\hbar$ ) for two values of the lattice distortion and the magnetic field. The topological Hall conductivity captures a negative value in both regimes  $\delta < 1$  and  $\delta > 1$ . On the other hand, Fig. 7 shows the magnetic field dependence of  $\kappa_{xy}$  which shows a symmetric sign reversal as the magnetic field changes sign.

We also note that a second-nearest neighbour antiferromagnetic interaction or magnon-phonon interaction may be present in real materials, which will probably enhance the thermal Hall conductivity. However, an external magnetic field is still required in order to produce a noncoplanar spin texture with nonzero  $\chi_{ijk}$ . Although the DM interaction is an intrinsic property of a material, if it is set to zero or negligible one finds that either a second-nearest neighbour antiferromagnetic interaction or an easy-plane anisotropy also stabilizes the coplanar/noncollinear Néel order. In this case it can be easily shown that both topological magnetic excitations and thermal Hall response are present at nonzero mag-

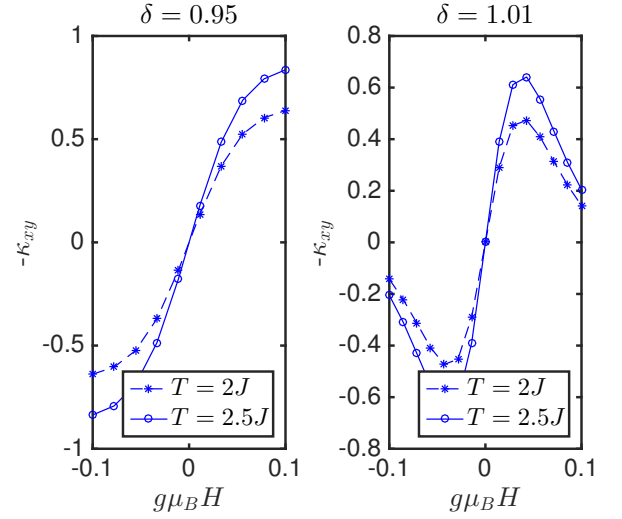


FIG. 7. Color online. Field dependence of the topological thermal Hall conductivity at low temperatures with  $D_{\perp}/J = 0.2$ .

netic field due to field-induced scalar spin chirality despite the absence of DM interaction. Therefore, antiferromagnetic kagomé materials with a weak (negligible) DM interaction can also possess a thermal Hall conductivity from the real space Berry curvature of the spin texture. Based on these results we believe that the scalar spin chirality induced either by the magnetic field or spontaneously (as in CSL phase) is the mechanism that gives rise to topological magnetic excitations with nonzero  $\kappa_{xy}$  in frustrated kagomé-lattice antiferromagnets as opposed to the DM interactions in collinear magnets.

## VI. CONCLUSION

In summary, we have studied topological magnetic excitations and thermal Hall effect induced by the real space Berry curvature of the spin texture on the distorted kagomé antiferromagnets applicable to vesignieite, edwardsite, and volborthite. In these magnetic systems, the lattice distortion is insufficient to lift the extensive classical degeneracy and therefore a zero energy mode persists in the low-energy magnetic excitations. The lack of inversion symmetry on the kagomé lattice allows a Dzyaloshinskii-Moriya (DM) interaction, which lifts the classical degeneracy and stabilizes the coplanar/noncollinear magnetic spin structure. We showed that although the distortion and DM interaction introduce gap magnetic excitations, the system remains topologically trivial with neither protected edge modes nor finite thermal Hall conductivity. By turning on an out-of-plane external magnetic field, we showed that a finite scalar spin chirality is induced from the topology of the spin configurations. This gives rise to a Berry curvature independent of the DM interaction. This topological Berry curvature persists in the chiral spin liquid (CSL)



phase due to the presence of the scalar spin chirality. In fact, starting from the Hubbard model with a magnetic field a  $t/U$  expansion at half filling gives a Heisenberg antiferromagnetic model with a scalar spin chiral interaction leading to CSL phase [56].

For a frustrated one-dimensional (1D) spin chain the DM interaction can be removed by a gauge transformation [70]. Most importantly, an ideal 1D system should not have a chiral noncoplanar magnetic order and scalar spin chirality should be absent. This suggests that the experimental result of thermal Hall response in volborthite can be best described using a distorted Heisenberg model as opposed to a frustrated alternating spin chain. An alternative approach is the Schwinger boson formalism, however in this formalism the scalar spin chirality does not appear explicitly on the kagomé antiferromagnets. Instead the DM interaction generates a magnetic flux [9, 71] even in the absence of an applied magnetic field leading to topological spin excitations. This is reminiscent of collinear ferromagnets and thus sharply contrast with the present results.

It is important to remark that the present topological spin excitations will occur in a wide range of kagomé antiferromagnetic models even without the magnetic field and DM interaction. For instance, the spin-1/2 Heisenberg model on the kagomé lattice with first-, second-, and third-neighbour interactions  $J_1$ ,  $J_2$ , and  $J_3$  exhibits different phases [57–59] in the absence of the magnetic field and DM interaction. One of the interesting phases is a cuboctahedron known as a *cuboc1* phase with 12 sublattices [72]. In this phase the spins on each triangle are coplanar, whereas the spins on the each hexagon have a noncoplanar magnetically ordered state with finite scalar spin chirality. In the *cuboc1* phase, the scalar spin chirality should generate topological spin excitations as presented here. The  $J_1$ - $J_2$ - $J_3$  model also exhibits a CSL phase with a nonzero scalar spin chirality [57–59] and we

expect topological excitations to persist in this regime.

As the DM interaction is intrinsic to the kagomé lattice, theoretical studies have established a quantum critical point (QCP) for spin-1/2 systems given by  $D_\perp^c/J \sim 0.1$  [31]. For  $D_\perp < D_\perp^c$  a QSL phase is predicted and for  $D_\perp > D_\perp^c$  an ordered coplanar/noncollinear Néel phase exists. From different experimental inspections, it is generally believed that both edwardsite and vesignieite are located in the ordered regime with  $0.1 < D_\perp/J < 0.16$  [37, 38], and there is a possibility that volborthite also belongs to the ordered regime at low temperatures. However, herbertsmithite  $\text{ZnCu}_3(\text{OH})_6\text{Cl}_2$  has  $D_\perp/J \sim 0.08$  and  $D_\parallel/J \sim 0.01$  (negligible) [32], thus it belongs to the QSL regime. In any case, materials with dominant  $D_\perp/J$  possess topological magnetic excitations and thermal Hall effect from real space Berry curvature induced by the spin texture as shown in this paper. The importance of this result is that the experimental determination of the DM interaction is not necessary for observing a finite thermal Hall conductivity in frustrated kagomé systems. This is of interest because there was no signal of DM interaction on the observed  $\kappa_{xy}$  in kagomé volborthite [3]. We believe that the results of this paper have shed more light on recent observation of thermal Hall conductivity in volborthite [3], and provides the mechanism for observing thermal Hall response in other distorted kagomé antiferromagnets such as vesignieite  $\text{BaCu}_3\text{V}_2\text{O}_8(\text{OH})_2$  and edwardsite  $\text{Cd}_2\text{Cu}_3(\text{SO}_4)_2(\text{OH})_6 \cdot 4\text{H}_2\text{O}$ .

## ACKNOWLEDGMENTS

The author would like to thank M. Yamashita, for elaborating on the experimental result of thermal Hall response in kagomé volborthite. Research at Perimeter Institute is supported by the Government of Canada through Industry Canada and by the Province of Ontario through the Ministry of Research and Innovation.

- 
- [1] Y. Onose, T. Ideue, H. Katsura, Y. Shiomi, N. Nagaosa, Y. Tokura, *Science* **329**, 297 (2010).
  - [2] Max Hirschberger, Robin Chisnell, Young S. Lee, and N. P. Ong, *Phys. Rev. Lett.* **115**, 106603 (2015).
  - [3] D. Watanabe, K. Sugii, M. Shimozaawa, Y. Suzuki, T. Yajima, H. Ishikawa, Z. Hiroi, T. Shibauchi, Y. Matsuda, M. Yamashita, *Proc. Natl. Acad. Sci. USA* **113**, 8653 (2016).
  - [4] H. Katsura, N. Nagaosa, and P. A. Lee, *Phys. Rev. Lett.* **104**, 066403 (2010).
  - [5] R. Matsumoto and S. Murakami, *Phys. Rev. Lett.* **106**, 197202 (2011); *Phys. Rev. B* **84**, 184406 (2011).
  - [6] T. Ideue, Y. Onose, H. Katsura, Y. Shiomi, S. Ishiwata, N. Nagaosa, and Y. Tokura, *Phys. Rev. B* **85**, 134411 (2012).
  - [7] L. Zhang, J. Ren, J. S. Wang, and B. Li, *Phys. Rev. B* **87**, 144101 (2013).
  - [8] A. Mook, J. Henk, and I. Mertig, *Phys. Rev. B* **90**, 024412 (2014); A. Mook, J. Henk, and I. Mertig, *Phys. Rev. B* **89**, 134409 (2014).
  - [9] H. Lee, J. H. Han, and P. A. Lee, *Phys. Rev. B* **91**, 125413 (2015).
  - [10] R. Chisnell, J. S. Helton, D. E. Freedman, D. K. Singh, R. I. Bewley, D. G. Nocera, and Y. S. Lee, *Phys. Rev. Lett.* **115**, 147201 (2015).
  - [11] Jung Hoon Han and Hyunyoung Lee, *J. Phys. Soc. Jpn.* **86**, 011007 (2017).
  - [12] Mook, A., Henk, J. and Mertig, *Phys. Rev. Lett.*, **117**, 157204 (2016).
  - [13] Y. Su, X. S. Wang, X. R. Wang, arXiv:1609.01500 (2016).
  - [14] A. L. Chernyshev and P. A. Maksimov, *Phys. Rev. Lett.* **117**, 187203 (2016).
  - [15] I. Dzyaloshinsky, *J. Phys. Chem. Solids* **4**, 241 (1958).
  - [16] T. Moriya, *Phys. Rev.* **120**, 91 (1960).

- [17] M. Z. Hasan and C. L. Kane, *Rev. Mod. Phys.* **82**, 3045 (2010).
- [18] X.-L. Qi and S.-C. Zhang, *Rev. Mod. Phys.* **83**, 1057 (2011).
- [19] Xiangang Wan, Ari M. Turner, Ashvin Vishwanath, and Sergey Y. Savrasov, *Phys. Rev. B* **83**, 205101 (2011).
- [20] A. A. Burkov and L. Balents, *Phys. Rev. Lett.* **107**, 127205 (2011).
- [21] S. A. Owerre, *J. Phys.: Condens. Matter* **28**, 235501 (2016).
- [22] S. A. Owerre, *J. Phys.: Condens. Matter* **28**, 386001 (2016).
- [23] S. A. Owerre, *J. Appl. Phys.* **120**, 043903 (2016).
- [24] Se Kwon Kim, Héctor Ochoa, Ricardo Zarzuela, Yaroslav Tserkovnyak, *Phys. Rev. Lett.* **117**, 227201 (2016).
- [25] David A. Huse and Andrew D. Rutenberg, *Phys. Rev. B* **45**, 7536(R) (1992).
- [26] A. B. Harris, C. Kallin, and A. J. Berlinsky, *Phys. Rev. B* **45**, 2899 (1992).
- [27] M. Elhajal, B. Canals, and C. Lacroix, *Phys. Rev. B* **66**, 014422 (2002).
- [28] Daniel Grohol, Daniel G. Nocera, and Dimitris Papoutsakis, *Phys. Rev. B* **67**, 064401 (2003).
- [29] D. Grohol, K. Matan, J.H. Cho, S.-H. Lee, J.W. Lynn, D.G. Nocera, Y.S. Lee, *Nature Materials* **4**, 323 (2005).
- [30] K. Matan, D. Grohol, D. G. Nocera, T. Yildirim, A. B. Harris, S. H. Lee, S. E. Nagler, and Y. S. Lee, *Phys. Rev. Lett.* **96**, 247201 (2006).
- [31] O. Cépas, C. M. Fong, P. W. Leung, and C. Lhuillier, *Phys. Rev. B* **78**, 140405(R) (2008).
- [32] A. Zorko, S. Nellutla, J. van Tol, L. C. Brunel, F. Bert, F. Duc, J.-C. Trombe, M. A. de Vries, A. Harrison, and P. Mendels, *Phys. Rev. Lett.* **101**, 026405 (2008).
- [33] H. Yoshida, Y. Michiue, E. Takayama-Muromachi, and M. Isobe, *J. Mater. Chem.* **22**, 18793 (2012).
- [34] A. Zorko, F. Bert, A. Ozarowski, J. van Tol, D. Boldrin, A. S. Wills, and P. Mendels, *Phys. Rev. B* **88**, 144419 (2013).
- [35] Y. Okamoto, H. Yoshida, and Z. Hiroi, *J. Phys. Soc. Jpn.* **78**, 033701 (2009).
- [36] R. H. Colman, F. Bert, D. Boldrin, A. D. Hillier, P. Manuel, P. Mendels, and A. S. Wills, *Phys. Rev. B* **83**, 180416(R) (2011).
- [37] J. A. Quilliam, F. Bert, R. H. Colman, D. Boldrin, A. S. Wills, and P. Mendels, *Phys. Rev. B* **84**, 180401(R) (2011).
- [38] M. Yoshida, Y. Okamoto, M. Takigawa, and Z. Hiroi, *J. Phys. Soc. Jpn.* **82**, 013702 (2013).
- [39] H. Yoshida, Y. Michiue, E. Takayama-Muromachi, and M. Isobe, *J. Mater. Chem.* **22**, 18793 (2012).
- [40] Hajime Ishikawa, Yoshihiko Okamoto, and Zenji Hiroi, *J. Phys. Soc. Jpn.* **82**, 063710 (2013).
- [41] Z. Hiroi, M. Hanawa, N. Kobayashi, M. Nohara, H. Takagi, Y. Kato and M. Takigawa, *J. Phys. Soc. Jpn.* **70**, 3377 (2001).
- [42] M. Yoshida, M. Takigawa, H. Yoshida, Y. Okamoto, and Z. Hiroi, *Phys. Rev. Lett.* **103**, 077207 (2009).
- [43] M. Yoshida, M. Takigawa, S. Kramer, S. Mukhopadhyay, M. Horvatic, C. Berthier, H. Yoshida, Y. Okamoto, Z. Hiroi, *J. Phys. Soc. Jpn.* **81**, 024703 (2012).
- [44] M. Yamashita, Private Communication.
- [45] H. Ishikawa, M. Yoshida, K. Nawa, M. Jeong, S. Krämer, M. Horvatic, C. Berthier, M. Takigawa, M. Akaki, A. Miyake, M. Tokunaga, K. Kindo, J. Yamaura, Y. Okamoto, Z. Hiroi, *Phys. Rev. Lett.* **114**, 227202 (2015).
- [46] Andreas P. Schnyder, Oleg A. Starykh, and Leon Balents, *Phys. Rev. B* **78**, 174420 (2008).
- [47] O. Janson, J. Richter, P. Sindzingre, H. Rosner, *Phys. Rev. B* **82**, 104434 (2010).
- [48] O. Janson, S. Furukawa, T. Momoi, P. Sindzingre, J. Richter, K. Held, *Phys. Rev. Lett.* **117**, 037206 (2016).
- [49] W. Apel, T. Yavors'kii, H.-U. Everts, *J. Phys.: Condens. Matter* **19**, 145255 (2007).
- [50] P. Sindzingre, arXiv:0707.4264.
- [51] Fa Wang, Ashvin Vishwanath, and Yong Baek Kim, *Phys. Rev. B* **76**, 094421 (2007).
- [52] P. H. Y. Li, R. F. Bishop, C. E. Campbell, D. J. J. Farnell, O. Götze, and J. Richter, *Phys. Rev. B* **86**, 214403 (2012).
- [53] V. Kalmeyer and R. B. Laughlin, *Phys. Rev. Lett.* **59**, 2095 (1987).
- [54] X. G. Wen, Frank Wilczek, and A. Zee, *Phys. Rev. B* **39**, 11413 (1989).
- [55] G. Baskaran, *Phys. Rev. Lett.* **63**, 2524 (1989).
- [56] B. Bauer, L. Cincio, B. P. Keller, M. Dolfi, G. Vidal, S. Trebst, A. W. W. Ludwig, *Nature Communications* **5**, 5137 (2014).
- [57] Shou-Shu Gong, Wei Zhu, Leon Balents, and D. N. Sheng, *Phys. Rev. B* **91**, 075112 (2015).
- [58] Alexander Wietek, Antoine Sterdyniak, and Andreas M. Läuchli, *Phys. Rev. B* **92**, 125122 (2015).
- [59] Samuel Bieri, Laura Messio, Bernard Bernu, and Claire Lhuillier, *Phys. Rev. B* **92**, 060407(R) (2015).
- [60] S.-S. Gong, W. Zhu, and D.N. Sheng, *Sci. Rep.* **4**, 6317 (2014).
- [61] Y. Taguchi, Y. Oohara, H. Yoshizawa, N. Nagaosa, Y. Tokura, *Science* **291**, 2573 (2001).
- [62] Y. Machida, S. Nakatsuji, Y. Maeno, T. Tayama, T. Sakakibara, and S. Onoda, *Phys. Rev. Lett.* **98**, 057203 (2007).
- [63] Y. Machida, S. Nakatsuji, S. Onoda, T. Tayama, and T. Sakakibara, *Nature*, **463**, 210 (2008).
- [64] Jian Zhou, Qi-Feng Liang, Hongming Weng, Y. B. Chen, Shu-Hua Yao, Yan-Feng Chen, Jinming Dong, and Guang-Yu Guo, *Phys. Rev. Lett.* **116**, 256601 (2016).
- [65] S. A. Owerre, arXiv:1608.00545 (2016).
- [66] Judit Romhányi, Karlo Penc, R. Ganesh, *Nature Communications* **6**, 6805 (2015).
- [67] T. Holstein and H. Primakoff, *Phys. Rev.* **58**, 1098 (1940).
- [68] A. Scheie, M. Sanders, J. Krizan, Y. Qiu, R.J. Cava, C. Broholm, *Phys. Rev. B* **93**, 180407 (2016).
- [69] R. Matsumoto, R. Shindou, and S. Murakami, *Phys. Rev. B* **89**, 054420 (2014).
- [70] Vladimir A. Zyuzin and Gregory A. Fiete, *Phys. Rev. B* **85**, 104417 (2012).
- [71] L. Messio, O. Cépas, and C. Lhuillier, *Phys. Rev. B* **81**, 064428 (2010).
- [72] J.-C. Dörmge, P. Sindzingre, C. Lhuillier, and L. Pierre, *Phys. Rev. B* **72**, 024433 (2005).

# Topological Magnetic Excitations on the Distorted Kagomé Antiferromagnets Supplemental Material

S. A. Owerre<sup>1,2</sup>

<sup>1</sup>Perimeter Institute for Theoretical Physics, 31 Caroline St. N., Waterloo, Ontario N2L 2Y5, Canada.

<sup>2</sup>African Institute for Mathematical Sciences, 6 Melrose Road, Muizenberg, Cape Town 7945, South Africa.

(Dated: December 13, 2024)

## I. MODEL HAMILTONIAN

We consider the Hamiltonian for kagomé antiferromagnets with DM interaction and Zeeman magnetic field given by

$$\mathcal{H} = \sum_{\langle i,j \rangle} [J_{ij} \mathbf{S}_i \cdot \mathbf{S}_j + \mathbf{D}_{ij} \cdot \mathbf{S}_i \times \mathbf{S}_j] - \mathbf{H} \cdot \sum_i \mathbf{S}_i, \quad (1)$$

where  $\mathbf{H} = h\hat{\mathbf{z}}$ ,  $h = g\mu_B H$  and  $\mathbf{D}_{ij} = -D_\perp \hat{\mathbf{z}}$ . This particular case of out-of-plane DM interaction is very common in most distorted kagomé antiferromagnetic materials. It is also interesting because topological magnetic excitations are not induced by the DM interaction as we will show. The presence of out-of-plane DM interactions breaks the complete SU(2) rotation symmetry down to U(1) symmetry about the  $z$ -axis. The classical energy is given by

$$e_0(\phi) = 2J(2 + \delta) [(1 - \cos \vartheta) \cos^2 \phi + \cos \vartheta] - 4D_\perp \sin^2 \phi \sin \vartheta (1 - \cos \vartheta) - 3h \cos \phi, \quad (2)$$

where  $e_0(\phi) = E(\phi)/NS^2$ ,  $N$  is the number of sites per unit cell, and  $\vartheta = \arccos(-1/2\delta)$  which is not exactly  $120^\circ$  for  $\delta \neq 1$ . The magnetic field is rescaled in unit of  $S$ . The minimization of  $e_0(\phi)$  yields the field-induced canting angle  $\cos \phi = h/h_s$  where

$$h_s = \frac{(1 - \cos \vartheta)}{3} [4J(2 + \delta) + 8D_\perp \sin \vartheta]. \quad (3)$$

The excitations above the classical ground state are obtained as follows. The procedure involves performing a rotation about the  $z$ -axis on the triad by the spin oriented angles  $\vartheta$  in order to achieve the coplanar configuration. As the out-of-plane magnetic field is turned on, we have to align the spins along the new quantization axis by performing a rotation about the  $y$ -axis by the field canting angle  $\phi$ . The total rotation matrix takes the form

$$\mathbf{S}_i = \mathcal{R}_z(\theta_i) \cdot \mathcal{R}_y(\phi) \cdot \mathbf{S}'_i, \quad (4)$$

where

$$\mathcal{R}_z(\theta_i) \cdot \mathcal{R}_y(\phi) = \begin{pmatrix} \cos \theta_i \cos \phi & -\sin \theta_i & \cos \theta_i \sin \phi \\ \sin \theta_i \cos \phi & \cos \theta_i & \sin \theta_i \sin \phi \\ -\sin \phi & 0 & \cos \phi \end{pmatrix}, \quad (5)$$

and  $\theta_i = \vartheta_{A,B,C}$ . In the following, we drop the prime in the rotated coordinate. At low temperatures accessible

experimentally, the noninteracting magnon model sufficiently describes the system. The corresponding Hamiltonian that contribute to noninteracting magnon model is given by

$$\mathcal{H}_J = \sum_{\langle i,j \rangle} J_{ij} [\cos \theta_{ij} \mathbf{S}_i \cdot \mathbf{S}_j + \sin \theta_{ij} \cos \phi \hat{\mathbf{z}} \cdot (\mathbf{S}_i \times \mathbf{S}_j)] \quad (6)$$

$$+ 2 \sin^2 \left( \frac{\theta_{ij}}{2} \right) (\sin^2 \phi S_i^x S_j^x + \cos^2 \phi S_i^z S_j^z),$$

$$\mathcal{H}_{DM} = D_\perp \sum_{\langle i,j \rangle} [\sin \theta_{ij} (\cos^2 \phi S_i^x S_j^x + S_i^y S_j^y) \quad (7)$$

$$+ \sin^2 \phi S_i^z S_j^z) - \cos \theta_{ij} \cos \phi \hat{\mathbf{z}} \cdot (\mathbf{S}_i \times \mathbf{S}_j)],$$

$$\mathcal{H}_h = -h \cos \phi \sum_i S_i^z, \quad (8)$$

where  $\theta_{ij} = \theta_i - \theta_j$ . At zero magnetic field, i.e.,  $\phi = \pi/2$ , the chiral interaction is absent in the magnon model despite the the presence of DM interaction. Hence, the system is topologically trivial at zero field. The magnetic-field-induced scalar spin chirality

$$\mathcal{H}_\chi = \sum_{i,j,k=\Delta} \chi_{ijk}, \quad (9)$$

originates from noncoplanar spin texture formed by the spin triad  $\mathbf{S}_i, \mathbf{S}_j, \mathbf{S}_k$ , where  $\chi_{ijk} = \mathbf{S}_i \cdot (\mathbf{S}_j \times \mathbf{S}_k)$ . It is well-known that  $\langle \chi_{ijk} \rangle$  can be nonzero even in the absence of magnetic ordering  $\langle \mathbf{S}_j \rangle = 0$ , e.g. in chiral spin liquid phase. This is a very crucial difference between collinear ferromagnets and antiferromagnets on the kagomé lattice. To obtain the magnon dispersions, we proceed as usual by introducing the Holstein Primakoff spin bosonic operators

$$S_i^z = S - a_i^\dagger a_i, \quad (10)$$

$$S_i^y = i\sqrt{\frac{S}{2}}(a_i^\dagger - a_i), \quad (11)$$

$$S_i^x = \sqrt{\frac{S}{2}}(a_i^\dagger + a_i), \quad (12)$$

where  $a_i^\dagger(a_i)$  are the bosonic creation (annihilation) operators. The noninteracting magnon tight binding Hamil-



tonian is given by

$$\mathcal{H} = S \sum_{\langle i,j \rangle} [G_{ij}^z (a_i^\dagger a_i + a_j^\dagger a_j) + G_{ij}^d (e^{-i\Phi_{ij}} a_i^\dagger a_j + h.c.)] \quad (13)$$

$$+ G_{ij}^o (a_i^\dagger a_j^\dagger + h.c.)] + h_\phi \sum_i a_i^\dagger a_i,$$

where

$$G_{ij}^z = -J_{ij} [\cos \theta_{ij} + 2 \cos^2 \phi \sin^2 (\theta_{ij}/2)] \quad (14)$$

$$- \mathcal{D}_\perp \sin^2 \phi \sin \theta_{ij},$$

$$G_{ij}^d = \sqrt{(G_{ij}^R)^2 + (G_{ij}^M)^2}, \quad (15)$$

$$G_{ij}^R = J_{ij} [\cos \theta_{ij} + \frac{2 \sin^2 \phi \sin^2 (\theta_{ij}/2)}{2}] \quad (16)$$

$$+ D_\perp \sin \theta_{ij} \left(1 - \frac{\sin^2 \phi}{2}\right),$$

$$G_{ij}^M = \cos \phi (J_{ij} \sin \theta_{ij} - D_\perp \cos \theta_{ij}), \quad (17)$$

$$G_{ij}^o = \frac{\sin^2 \phi}{2} (2J_{ij} \sin^2 (\theta_{ij}/2) - D_\perp \sin \theta_{ij}), \quad (18)$$

and  $h_\phi = h \cos \phi$ . The fictitious magnetic flux or solid angle subtended by three noncoplanar spins is given by  $\tan \Phi_{ij} = G_{ij}^M / G_{ij}^R$ . We clearly see that  $\Phi_{ij}$  is nonzero in the absence of DM interaction. It should be noted that the  $\mathbf{Q} = \mathbf{0}$  magnetic structure that can be stabilized by other means as mentioned in the text. In momentum space we obtain

$$\mathcal{H} = S \sum_{\mathbf{k}, \alpha, \beta} (2\mathcal{M}_{\alpha\beta}^z \delta_{\alpha\beta} + 2\mathcal{M}_{\alpha\beta}^d) a_{\mathbf{k}\alpha}^\dagger a_{\mathbf{k}\beta} \quad (19)$$

$$+ \mathcal{M}_{\alpha\beta}^o (a_{\mathbf{k}\alpha}^\dagger a_{-\mathbf{k}\beta}^\dagger + a_{\mathbf{k}\alpha} a_{-\mathbf{k}\beta}),$$

where  $\alpha, \beta = A, B, C$  and the coefficients are given by

$$\mathcal{M}^z = \text{diag}(\zeta_{AA}, \zeta_{BB}, \zeta_{CC}), \quad (20)$$

with  $\zeta_{AA} = G_{AB}^z + G_{CA}^z + h_\phi/2$ ,  $\zeta_{BB} = \zeta_{CC} = G_{AB}^z + G_{BC}^z + h_\phi/2$ . In the undistorted limit  $\delta \rightarrow 1$ ,  $\zeta_{AA} = \zeta_{BC} = \zeta_{CA}$ . For the distorted case  $\delta \neq 1$  the situation is different. We have  $\zeta_{AA} > \zeta_{BC}$ ,  $\zeta_{CA}$  for  $\delta < 1$  and  $\zeta_{AA} < \zeta_{BC}$ ,  $\zeta_{CA}$  for  $\delta > 1$ .

$$\mathcal{M}^d = \begin{pmatrix} 0 & \gamma_{AB}^d e^{-i\Phi_{AB}} & \gamma_{CA}^d e^{i\Phi_{CA}} \\ \gamma_{AB}^{*d} e^{i\Phi_{AB}} & 0 & \gamma_{BC}^d e^{-i\Phi_{BC}} \\ \gamma_{CA}^{*d} e^{-i\Phi_{CA}} & \gamma_{BC}^{*d} e^{i\Phi_{BC}} & 0 \end{pmatrix}, \quad (21)$$

$$\mathcal{M}^o = \begin{pmatrix} 0 & \gamma_{AB}^o & \gamma_{CA}^o \\ \gamma_{AB}^{*o} & 0 & \gamma_{BC}^o \\ \gamma_{CA}^{*o} & \gamma_{BC}^{*o} & 0 \end{pmatrix}, \quad (22)$$

where  $\gamma_{AB}^d = G_{AB}^d \cos k_1$ ,  $\gamma_{BC}^d = G_{BC}^d \cos k_2$ ,  $\gamma_{CA}^d = G_{CA}^d \cos k_3$ ;  $\gamma_{AB}^{*o} = G_{AB}^o \cos k_1$ ,  $\gamma_{BC}^{*o} = G_{BC}^o \cos k_2$ ,  $\gamma_{CA}^{*o} = G_{CA}^o \cos k_3$ .  $k_i = \mathbf{k}_i \cdot \mathbf{e}_i$ , and  $\mathbf{e}_1 = (-1/2, -\sqrt{3}/2)$ ,  $\mathbf{e}_2 = (1, 0)$ ,  $\mathbf{e}_3 = (-1/2, \sqrt{3}/2)$ . The Hamiltonian can be written as

$$\mathcal{H} = S \sum_{\mathbf{k}} \Psi_{\mathbf{k}}^\dagger \mathcal{H}(\mathbf{k}) \Psi_{\mathbf{k}} - \text{const.}, \quad (23)$$

where  $\Psi_{\mathbf{k}}^\dagger = (b_{\mathbf{k}A}^\dagger, b_{\mathbf{k}B}^\dagger, b_{\mathbf{k}C}^\dagger, b_{-\mathbf{k}A}, b_{-\mathbf{k}B}, b_{-\mathbf{k}C})$ , and

$$\mathcal{H}(\mathbf{k}) = \begin{pmatrix} \mathcal{M}^z + \mathcal{M}^d & \mathcal{M}^o \\ \mathcal{M}^o & \mathcal{M}^z + \mathcal{M}^d \end{pmatrix}. \quad (24)$$

## II. MATRIX DIAGONALIZATION

The Hamiltonian is diagonalized by the generalized Bogoliubov transformation  $\Psi_{\mathbf{k}} = \mathcal{P}_{\mathbf{k}} Q_{\mathbf{k}}$ , where  $\mathcal{P}_{\mathbf{k}}$  is a  $2N \times 2N$  paraunitary matrix and  $Q_{\mathbf{k}}^\dagger = (Q_{\mathbf{k}}^\dagger, Q_{-\mathbf{k}})$  with  $Q_{\mathbf{k}}^\dagger = (\beta_{\mathbf{k}A}^\dagger, \beta_{\mathbf{k}B}^\dagger, \beta_{\mathbf{k}C}^\dagger)$  being the quasiparticle operators. The matrix  $\mathcal{P}_{\mathbf{k}}$  satisfies the relations,

$$\mathcal{P}_{\mathbf{k}}^\dagger \mathcal{H}(\mathbf{k}) \mathcal{P}_{\mathbf{k}} = \mathcal{E}_{\mathbf{k}} \quad (25)$$

$$\mathcal{P}_{\mathbf{k}}^\dagger \tau_3 \mathcal{P}_{\mathbf{k}} = \tau_3, \quad (26)$$

where  $\mathcal{E}_{\mathbf{k}} = \text{diag}(\omega_{\mathbf{k}\alpha}, \omega_{-\mathbf{k}\alpha})$ ,  $\tau_3 = \text{diag}(\mathbf{I}_{N \times N}, -\mathbf{I}_{N \times N})$ , and  $\omega_{\mathbf{k}\alpha}$  are the energy eigenvalues. From Eq. 26 we get  $\mathcal{P}_{\mathbf{k}}^\dagger = \tau_3 \mathcal{P}_{\mathbf{k}}^{-1} \tau_3$ , and Eq. 25 is equivalent to saying that we need to diagonalize the Hamiltonian  $\mathcal{H}'(\mathbf{k}) = \tau_3 \mathcal{H}(\mathbf{k})$ , whose eigenvalues are given by  $\tau_3 \mathcal{E}_{\mathbf{k}}$  and the columns of  $\mathcal{P}_{\mathbf{k}}$  are the corresponding eigenvectors. The eigenvalues of this Hamiltonian cannot be obtained analytically except at zero field. The paraunitary operator  $\mathcal{P}_{\mathbf{k}}$  defines a Berry curvature given by

$$\Omega_{ij;\alpha}(\mathbf{k}) = -2\text{Im}[\tau_3(\partial_{k_i} \mathcal{P}_{\mathbf{k}\alpha}^\dagger) \tau_3(\partial_{k_j} \mathcal{P}_{\mathbf{k}\alpha})]_{\alpha\alpha}, \quad (27)$$

with  $i, j = \{x, y\}$  and  $\mathcal{P}_{\mathbf{k}\alpha}$  are the columns of  $\mathcal{P}_{\mathbf{k}}$ . In this form, the Berry curvature simply extracts the diagonal components which are the most important. From Eq. 25 the Berry curvature can be written alternatively as

$$\Omega_{ij;\alpha}(\mathbf{k}) = -2 \sum_{\alpha' \neq \alpha} \frac{\text{Im}[\langle \mathcal{P}_{\mathbf{k}\alpha} | v_i | \mathcal{P}_{\mathbf{k}\alpha'} \rangle \langle \mathcal{P}_{\mathbf{k}\alpha'} | v_j | \mathcal{P}_{\mathbf{k}\alpha} \rangle]}{(\omega_{\mathbf{k}\alpha} - \omega_{\mathbf{k}\alpha'})^2}, \quad (28)$$

where  $\mathbf{v} = \partial \mathcal{H}'(\mathbf{k}) / \partial \mathbf{k}$  defines the velocity operators. The Berry curvature is related to the solid angle  $\Omega(\mathbf{k}) \propto \Phi$  and the Chern number is defined as,

$$\mathcal{C}_\alpha = \frac{1}{2\pi} \int_{BZ} dk_x dk_y \Omega_{xy;\alpha}(\mathbf{k}). \quad (29)$$

It can be shown that the Chern numbers are related to the scalar-chirality-induced fictitious flux  $\Phi$  as  $\mathcal{C}_1 = 0$ ,  $\mathcal{C}_2 = -\text{sgn}(\sin(\Phi))$ ,  $\mathcal{C}_3 = \text{sgn}(\sin(\Phi))$ , where

$$\sin(\Phi) = \frac{1}{2} \chi_{ijk}. \quad (30)$$